Title
Osmotically driven drug delivery through remote-controlled magnetic nanocomposite membranes

Journal
Biomicrofluidics, 9(5)

ISSN
1932-1058

Authors
Zaher, A
Li, S
Wolf, KT
et al.

Publication Date
2015-09-01

DOI
10.1063/1.4931954

Peer reviewed

Osmotically driven drug delivery through remote-controlled magnetic nanocomposite membranes

A. Zaher,[1,a),b)] S. Li,[2,a)] K. T. Wolf,[3] F. N. Pirmoradi,[3] O. Yassine,[4] L. Lin,[3] N. M. Khashab,[2] and J. Kosel[4,b)]
[1]*School of Engineering, University of British Columbia, Kelowna, British Columbia V1V 1V7, Canada*
[2]*Smart Hybrid Materials (SHMs) Lab, Advanced Membranes and Porous Materials Center, King Abdullah University of Science and Technology (KAUST), Thuwal 23955, Saudi Arabia*
[3]*Department of Mechanical Engineering, University of California at Berkeley, California 94720, USA*
[4]*Computer, Electrical and Mathematical Science and Engineering Division, King Abdullah University of Science and Technology (KAUST), Thuwal 23955, Saudi Arabia*

(Received 10 June 2015; accepted 17 September 2015; published online 29 September 2015)

Implantable drug delivery systems can provide long-term reliability, controllability, and biocompatibility, and have been used in many applications, including cancer pain and non-malignant pain treatment. However, many of the available systems are limited to zero-order, inconsistent, or single burst event drug release. To address these limitations, we demonstrate prototypes of a remotely operated drug delivery device that offers controllability of drug release profiles, using osmotic pumping as a pressure source and magnetically triggered membranes as switchable on-demand valves. The membranes are made of either ethyl cellulose, or the proposed stronger cellulose acetate polymer, mixed with thermosensitive poly(*N*-isopropylacrylamide) hydrogel and superparamagnetic iron oxide particles. The prototype devices' drug diffusion rates are on the order of 0.5–2 μg/h for higher release rate designs, and 12–40 ng/h for lower release rates, with maximum release ratios of 4.2 and 3.2, respectively. The devices exhibit increased drug delivery rates with higher osmotic pumping rates or with magnetically increased membrane porosity. Furthermore, by vapor deposition of a cyanoacrylate layer, a drastic reduction of the drug delivery rate from micrograms down to tens of nanograms per hour is achieved. By utilizing magnetic membranes as the valve-control mechanism, triggered remotely by means of induction heating, the demonstrated drug delivery devices benefit from having the power source external to the system, eliminating the need for a battery. These designs multiply the potential approaches towards increasing the on-demand controllability and customizability of drug delivery profiles in the expanding field of implantable drug delivery systems, with the future possibility of remotely controlling the pressure source. © *2015 AIP Publishing LLC*. [http://dx.doi.org/10.1063/1.4931954]

I. INTRODUCTION

The field of drug delivery is of increasing interest amongst academic and industrial researchers seeking to optimize methods for localized, passive, smart, and remotely triggerable, on-demand drug delivery systems.[1–11] Functionalized organic composites that react to external stimuli such as heat, light, pH, ultrasound, or magnetic fields are of particular interest for

[a)]A. Zaher and S. Li contributed equally to this work.
[b)]Authors to whom correspondence should be addressed. Electronic addresses: amirzaher@alumni.ubc.ca and jurgen.kosel@kaust.edu.sa

specific biomedical applications.[12,13] For example, poly(*N*-isopropylacrylamide) (PNIPAM) has been utilized as a thermosensitive polymer in drug delivery systems by grafting with other polymers or inorganic particles,[14–17] in the forms of nanoparticles,[18,19] micelles,[20] liposomes,[21,22] or core-shell structures.[23,24] The hydrogel presents different volume phases and hydrophilicity at a transition temperature, known as the lower critical solution temperature, which determines the hydrogel's swelling state by influencing the formation of H-bonds among polymer networks. Below this critical temperature, PNIPAM is highly hydrophilic and swells in an aqueous environment due to intermolecular H-bonds with water. Above the critical temperature, it becomes relatively hydrophobic and shrinks in volume, as the intermolecular H-bonds tend to break while the intramolecular ones are preferred and formed. PNIPAM-based membranes have been shown to be viable control switches as gates for on-off drug release profiles.[12,25] On the one hand, they can occupy the diffusion pathways in films and limit mass transport below the lower critical solution temperature. On the other hand, they can shrink in size above the lower critical solution temperature, allowing for higher diffusion rates. The thermosensitive controllability can be tailored to allow for magnetic-triggering by incorporating magnetic nanoparticles into the drug delivery system,[12,14–17,25] where magnetic particles such as Fe_3O_4 convert energy from an alternating magnetic field to thermal energy, by Néel and Brownian relaxations, and transfer the heat to induce the shrinkage of the hydrogel.

Implantable devices are playing an increasingly important role in therapeutic treatments. Over the past several years, significant advancements have been made with regards to the synthesis and tunability of functionalized drug carriers, switches, membranes, containers, pumps, and valves.[1,3,5–8,11–13,26–30] State of the art implantable micro-devices include reservoir-based systems, controlled-release microchips, and various electrically powered microsystems.[1,2,10,31] Osmotic pumps present a convenient and reliable cost-effective drug delivery method capable of replacing repeated injections of soluble and poorly soluble drugs[32,33] for the treatment of chronically debilitating diseases.[3,4,34–36] These marketed pumps use the principle of osmotic pressure for the delivery of pharmaceutical ingredients at a predetermined rate[37] and eliminate the need for frequent handling and injections, without external connectors. For example, Duros brand pumps have been used for parenteral therapy, over periods of days to years, for both local and systemic drug delivery.[4] Osmotic drug delivery systems have also been used in animal testing related to the treatment of central nervous system disorders,[38,39] spinal cord injuries,[40] cerebral malaria,[41] peripheral arterial disease,[42] Parkinson's disease,[43] to name a few, as well as in discrete and daily dosing of anabolic osteoporosis medication via wirelessly controlled microchips implanted in human patients.[35] These state-of-art osmotic drug devices are limited to constant drug release, without real-time controllability or variable dosing.

There has been an increased interest in the development of remotely modulated drug delivery from implantable devices. Examples of the need for such systems, where short bursts of increased delivery are highly optimal, include insulin delivery and osteoporosis therapy.[35,44] For these cases, a lower, sustained bias delivery rate, driven by a pressure source, would address the need for continuous treatment. This is then supplemented by intermittent on-demand rate increases. Similarly, switchable transdermal nicotine delivery rates are pursued to address the varying therapeutic demand levels for nicotine cessation treatments.[45] Chronic diseases that present symptom flare up, including diabetes,[46,47] hemophilia,[48,49] hypertension,[50] high cholesterol,[51] asthma,[52] seasonal allergies,[53] and chronic seizures,[54] may potentially be addressed using variable dosing. Furthermore, in the case of diseases that affect specific locations in the body (e.g., internal bleeding at joints in hemophiliacs), localized device implantation can allow for significant reductions in the required drug mass delivery by bypassing untargeted organs such as the stomach, small intestine, liver, and kidney, which cause unnecessary loss of drugs.

This work proposes and demonstrates controllable drug delivery from osmotically powered systems using PNIPAM-based membranes as the valves and embedded magnetic nanoparticles as the heating elements. By utilizing a magnetic membrane as the control mechanism, the device benefits from having the power source external to the system, and the elimination of the need for an on-chip battery. Different membrane material designs have been investigated using a simulation model and experimentally characterized.

II. METHODS

A. Device design

The main design consists, from bottom to top, of (i) an osmotic pump that resides underneath (ii) a donor chamber containing the model drug, 1 mg/mL of Rhodamine-B (RhB), (iii) a magnetically triggered nanocomposite membrane separating the donor chamber from (iv) a receptor chamber containing pure water, as illustrated in Fig. 1(a). The osmotic pump contains NaCl salt and, when its water inlet is wetted, its volume expands with the influx of water against its flexible poly(dimethylsiloxane) (PDMS) membrane, pressurizing the donor solution towards the receptor. The water inlet membrane is made of pure ethyl cellulose (EC), permeable to water and preventing the loss of NaCl. The nanocomposite membrane consists of either EC or cellulose acetate (CA) as a matrix with embedded PNIPAM and superparamagnetic iron oxide (SPIO) particles. When an alternating magnetic field is applied, the SPIO particles generate heat via magnetic losses, which results in the shrinkage of the thermosensitive PNIPAM (Fig. 1(b)). This increase in porosity of the membrane allows for higher diffusion rates of RhB,

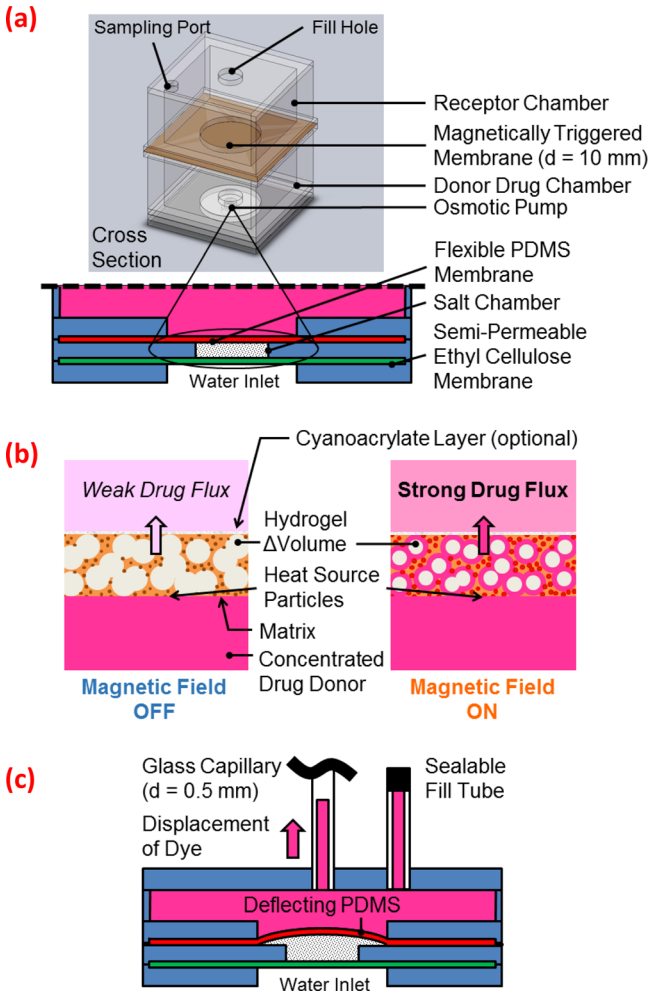

FIG. 1. (a) Schematic diagram of the drug delivery system with magnetic composite membrane and osmotic pump. The structural material is made of laser-etched and chloroform bonded PMMA stacks. (b) PNIPAM hydrogel undergoing swelling (left) and shrinking (right) before and during the application of an AC magnetic field. SPIO particles react to the AC magnetic field to generate heat and the shrinkage of the PNIPAM hydrogel. This shrinkage induces the large flux shown. (c) Test setup used to characterize the operation of the osmotic pump. The drug reservoir is filled using a sealable fill tube, and the initial level of dye in the glass capillary is recorded. After the activation of the osmotic pump, the level of the dye is recorded over time to calculate the pumped volume.

through the membrane and into the receptor chamber. A combination of increased porosity and osmotic pressure results in higher RhB dosing. The effect of a cyanoacrylate layer on top of the nanocomposite membrane (Fig. 1(b)) on the drug release is also studied to address the need for delivery rate reduction when applications depend on a small release of highly concentrated, high potency, drug solutions.

The main body of the device is $20 \times 20 \times 26\,\text{mm}^3$ and is made of six 1 mm and two 10 mm thick laser-etched and chloroform bonded poly(methyl 2-methylpropenoate) (PMMA) stacks (Fig. 1(a)). Both the donor and receptor chambers have a volume of 2.3 mL, in order to have enough solution for analysis. The 5 mm diameter fill hole on top of the system is used to fill the receptor with water, and the 2.5 mm diameter sampling port is used to extract fluid samples for solution analysis.

The donor chamber has two 1 mm fill holes drilled through one wall (one used for RhB intake and the other for air outflow) for accurate filling of the chamber with RhB and evacuation of air bubbles. The nanocomposite membrane has an opening of 10 mm in diameter. The osmotic pump consists of three 1 mm thick layers of PMMA sheets (Fig. 1(a) bottom) that hold a semi-permeable membrane made of 20 μm-thick ethyl cellulose, above which is the salt chamber, 2 mm in diameter and 1 mm in height containing powdered NaCl, which is in turn underneath a 63 μm-thick PDMS membrane, insulating the NaCl from the donor chamber. Fig. 1(c) shows the schematic diagram of an assembled osmotic pump with a fill tube and a glass capillary, 0.5 mm in diameter, attached to the donor drug reservoir for basic characterizations of the pump operation. The vertical displacement of the dye is measured over time and data are collected to determine the pump flow rates before (priming phase) and during drug delivery operations. A large osmotic gradient occurs between the semi-permeable membrane and the salt when the pump is wetted,[4] and water is continuously drawn through the pump's EC semi-permeable membrane due to the concentration differences. Only the PDMS membrane is in direct contact with the RhB solution in the donor cell. When the pump is activated, the volume of the salt chamber expands and pushes against the donor cell solution by deflecting the PDMS, hence increasing the donor pressure.

B. Fabrication of the osmotic pump

A 20 μm-thick, semi-permeable membrane made solely of ethyl cellulose is cast on a glass slide using a micrometer adjustable film applicator (Sheen Instruments, Elektron Technology Group, Cambridge, UK). This membrane is then released in water and left to dry while compressed between filter paper sheets (>16 h). A buffered oxide etch and Piranha Etch treated silicon wafer is used to spin coat 63 μm-thick PDMS, from which membranes of approximately 10–15 mm in diameter are laser cut as the deformable pump membrane. Adhesive (Loctite 401 glue) is used to ensure watertight sealing between osmotic NaCl chamber, donor, and exterior. The osmotic NaCl chamber is filled with finely powdered NaCl, and sealed from the pump's bottom with an adhered ethyl cellulose membrane. The PMMA layer with a water intake hole of 4 mm in diameter at the bottom defines the water inlet. When attached to the donor chamber, an additional viscous PMMA-chloroform mixture is used to prevent possible leakages of the system. Upon evaporation of the chloroform content, the remaining structural material is composed only of PMMA.

C. Fabrication of magnetic nanocomposite membranes

1. PNIPAM hydrogels

The PNIPAM hydrogels are prepared by copolymerization of NIPAm, *N*-isopropylmethacrylamide (NIPMAm) and acrylamide (AAm) by adding 300 mL de-ionized water, 4 g NIPAm (35.3 mmol), 7.44 g NIPMAm (58.5 mmol), 0.5 g AAm (7.0 mmol), and 0.78 g bis-acrylamide (5.6 mmol) crosslinker at 40 °C under continuous stirring and nitrogen purging. After 1 h, the reaction is initiated by adding 1 g potassium persulfate (3.7 mmol) and increasing the temperature to 70 °C. The mixture is kept at this temperature for 12 h to obtain a white suspension,

which is then allowed to cool at ambient conditions. To remove the unreacted monomers and small polymer molecules, this mixture is purified by dialysis in de-ionized water for 2 days using a 25 kDa MWCO dialysis bag. White PNIPAM hydrogel powders are obtained by lyophilization. The volume phase transition temperature of the PNIPAM hydrogels is observed by monitoring the absorbance of PNIPAM aqueous suspension on a UV/Vis spectrum (UV-Vis-NIR system, Cary 5000, Agilent, Santa Clara, CA) under different temperatures. From 35 °C to 50 °C, the temperature is gradually increased by 1 °C increments, and each temperature is held for 10 min before the absorbance at 500 nm (A_{500}) is recorded. The A_{500}-T curve is established to determine the transition temperature.

2. Superparamagnetic iron oxide nanoparticles

The synthesis of Fe_3O_4 SPIO particles is performed using a high-temperature organic-phase decomposition method.[55] Briefly, $Fe(acac)_3$ (2.0 mmol), 1,2-hexadecanediol (10.0 mmol), oleic acid (6.0 mmol), oleylamine (6.0 mmol), and 20 mL phenyl ether (126 mmol) are mixed under nitrogen purging. The mixture is heated to 200 °C for 2 h and then to 300 °C for another 1 h. After the chemical reaction, the mixture is allowed to cool at ambient conditions, followed by precipitation in 40 mL (685 mmol) of ethanol. To purify the resulting precipitate, the solution is dissolved into hexane with 0.05 mL (0.157 mmol) oleic acid and 0.05 mL (0.152 mmol) oleylamine, and then centrifuged at 4000 rpm for 15 min to remove any undispersed residue. The SPIO dispersion is precipitated again in ethanol and re-dispersed into hexane for storage or use.

3. Magnetic nanocomposite membranes

The nanocomposite membranes are based on either CA or EC, used as the porous matrices, with inter-dispersed PNIPAM hydrogel and SPIO particles. Membranes are fabricated for individual characterizations (diffusion testing by direct heating in two-chamber glass diffusion cells), and for integration in the drug delivery devices. These membranes have thicknesses between 16 μm and 21 μm after being cast-set (using film applicator). The nanocomposite membranes are fabricated by casting the desired mixture dispersion on glass slides. The EC-PNIPAM-SPIO membrane is fabricated by adding 1 g of 8 wt. % EC in ethanol with 40 mg of PNIPAM while stirring for 12 h to obtain a homogeneous mixture. The SPIO dispersion (containing 75 mg SPIO) is precipitated in an equal volume of ethanol and washed with ethanol before it is mixed with the previous dispersion. The fabrication of the CA-PNIPAM-SPIO membrane follows the same procedure, except that 10 wt. % CA in acetone is used in the mixture. All membranes are allowed to dry at ambient conditions (>16 h) and observed by scanning electron microscopy (Fig. 2) to determine the membranes' equivalent thicknesses and morphologies. The average thicknesses are obtained as the mean value of 8 different positions along the cross-sections as listed in Table I.

4. Cyanoacrylate vapour deposition

Vapor deposition of inert, medically implementable, cyanoacrylate[56,57] is used to drastically reduce the drug delivery rate. The deposition process consists of covering one side of the nanocomposite membrane with a $10 \times 10 \times 5\,mm^3$ hollow, cube-shaped, bottomless plastic enclosure. The enclosure has a 5 mm diameter ventilation hole on its top side. A 0.08 mL volume of cyanoacrylate is spread along the bottom of the four inner sides of the enclosure using a needle tip, ensuring a well distributed vapor source. The setup is left undisturbed for over 16 h (room temperature). As the cyanoacrylate vapor cures and polymerizes, its vapor deposits on the surface of the membrane. This creates a permeable barrier, whose permeability is a function of the amount of cyanoacrylate placed on the enclosure's inner sides. The purpose of the 5 mm hole is to allow the un-deposited vapors to exit the enclosure as they diffuse atop and past the membrane.

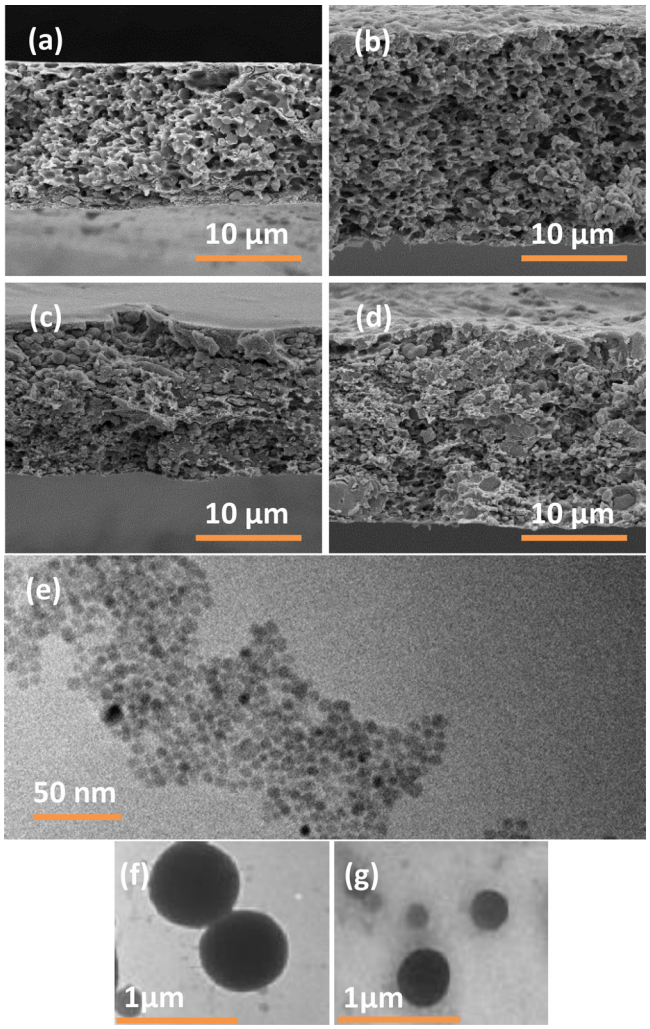

FIG. 2. Scanning electron microscopy images of the cross-sections of different nanocomposite membranes, (a) EC with PNIPAM, (b) EC with PNIPAM and SPIO particles, (c) CA with PNIPAM, (d) CA with PNIPAM and SPIO particles. Transmission electron microscopy images of (e) synthesized 8 nm SPIO particles, (f) PNIPAM particles in water, 800 nm at 37 °C and (g) 400 nm at 45 °C (using direct heating).

5. Mechanical characterization of membrane types

The ASTM D 790-07 standard test method is used to mechanically characterize EC-PNIPAM and CA-PNIPAM membranes, as they yield under a 3-point loading system (Instron, Illinois Tool Works, Glenview, IL). The mean flexural stress of five samples at the breaking point is measured for both dry and wet conditions. Membranes are broken into approximately 5 mm wide and 10 mm long segments. The formula for a rectangular sample under a load in a 3-point loading system is given by

TABLE I. Thickness measurements of different nanocomposite membranes after casting and curing.

Membrane types	Thickness
EC with PNIPAM	15.48 ± 1.43 μm
EC with PNIPAM and SPIO	18.78 ± 2.03 μm
CA with PNIPAM	12.97 ± 2.12 μm
CA with PNIPAM and SPIO	18.73 ± 3.45 μm

$$\sigma = \frac{3FL}{2bd^2}, \tag{1}$$

where F is the load force at the fracture point (N), L is the length of the span between the two supports on which the sample rests, b is the width of the sample (mm), and d is the thickness (mm).

D. Modeling and numerical simulations

Finite element simulation software (COMSOL) is used to simulate the drug delivery device focusing on the osmotically pressurized cyanoacrylate treated EC membrane with PNIPAM hydrogel and SPIO particles. The numerical model is developed based on three modules in the software: fluid-structure interaction (FSI) for the flexible PDMS, free flow and flow through porous media for the magnetically triggered membrane, and species transport through free and porous media for the RhB diffusion. The FSI module combines the Navier-Stokes equation that applies to water with the structural mechanics equation for isotropic linearly elastic material that is nearly incompressible (PDMS), while Brinkman's equation is utilized for porous regions. The transport of RhB solution through porous and free media can be solved with a module in COMSOL. In this work, the governing equation of the module is transferred to a mathematical module and simplified for the simulation (see supplementary material SA-SF)[63]

$$\varepsilon \frac{\partial \mathrm{c}}{\partial \mathrm{t}} + \nabla \cdot (\mathrm{c}\boldsymbol{u}) = \nabla \cdot \left(\left(\varepsilon^{\frac{4}{3}} \mathrm{D} \right) \nabla \mathrm{c} \right), \tag{2}$$

where ε is the porosity, c is the concentration, $\boldsymbol{u}$ is the velocity profile, and D is the diffusion coefficient of the diffusing species.

An analytical approximation is used to find the return force-induced pressure from the osmotic chamber on the flexible PDMS membrane, P_{PDMS}. The analytical equation for this applied pressure on the PDMS membrane is derived from two basic equations that describe the elastic deflection of a membrane and the fluid flow through a semi-permeable membrane, namely, the equation of deflection of a circular plate with clamped edges and under uniform lateral load,[58] and Darcy's Law.[59] By combining these and the boundary conditions (see supplementary material SG),[63] an approximation of the applied pressure on the PDMS membrane is derived

$$\mathrm{P}_{PDMS} = \alpha \mathrm{V}^3 + \frac{\mu \mathrm{h}}{kA} \dot{V}. \tag{3}$$

In Equation (3),

- $\mathrm{P}_{\mathrm{PDMS}}$ is the applied pressure on the PDMS membrane by the osmotic chamber in the pump.
- α is a parameter determined when solely examining the PDMS membrane deflection.
- V is the fluid volume displaced due to PDMS deflection.
- μ is the dynamic viscosity of the fluid.
- h is the thickness of the magnetically responsive membrane.
- k is the mechanical permeability of the magnetically responsive membrane.
- A is the cross-sectional area of the magnetically responsive membrane.
- $\dot{V}$ is the rate of volume displacement over time.

The second term appears only with the existence of the magnetically responsive membrane, while the first term represents the contribution of the osmotic pump's displaced volume via the deflection of the PDMS membrane.

An approximated applied pressure on the PDMS membrane, used to simulate its behavior alone, shows an interesting behavior of the input pressure profile. Since the magnetic membrane's permeability is low in general, the small displacement of the PDMS membrane reduces the influence of the $\alpha \mathrm{V}^3$ term on P_{PDMS}, causing the pressure profile applied onto the donor

chamber to be dominated by the volume displacement rate $\dot{V}$ through the magnetic membrane and the permeability k of the magnetic membrane in the second term.

The approximation of the permeability of the magnetic membrane is based on work done on fluid transport and permeability of water vapor through EC.[60] From such a basis, the magnitude of P_{donor} is determined (see supplementary material SH).[63] The permeability of the magnetic membrane is calibrated with this applied pressure, and the permeability difference between the magnetically activated and deactivated states is approximated by comparing the two states (magnetic field on and off), which gives a ratio of the magnetic membrane's permeability values for the two states (see supplementary material SI).[63]

The simulation process is divided into four parts, namely, (1) direct pressure test (PDMS membrane behavior without simulating osmotic process), (2) magnetic membrane porosity calibration, (3) magnetic membrane permeability calibration, and (4) simulation of the full osmotic pump and magnetic membrane assembly.

E. Device characterization

We report two different devices in this study, using either a CA membrane or a cyanoacrylate treated EC membrane, each containing PNIPAM hydrogel and SPIO particles, and undergoing similar test conditions. The device prototype using a CA membrane was tested over a span of 10.5 h, split into four test stages. In the first stage, the donor and receptor are carefully loaded with RhB and DI water, respectively. The donor's fill holes are then sealed with several layers of PMMA-chloroform mixture that quickly dries while under a fume extraction system. The device is left upright at room temperature on a dry platform with the deactivated osmotic pump on the bottom for a total of 3 h, after which a small amount of the receptor fluid is immediately analyzed via UV spectrophotometry to determine the total amount of RhB initially diffused, then slowly re-injected into the receptor (via the sampling port) such that the membrane does not experience any excess force. UV analysis is conducted in such a manner for every device. With the diffusion process fully initiated and stable, this first measurement is used as the zero point for a second room temperature rate. In the second stage, while maintaining the same orientation as before, the device is placed in the center of a vertically oriented magnetic solenoid of a water cooled 3 kW inductive heater (Induktive Erwärmungsanlagen GmbH, Austria), and cycled through approximately three, 1 h long on-off magnetization periods, each period including 30 min of exposure to a 62 mT, 450 kHz magnetic field, followed by 30 min with the field off, totaling 3 h prior to UV analysis. Depending on the application, the exposure time within this magnetization period could be adjusted. The magnetic field generated by the inductive heater is measured using a pickup coil of known area, connected to an oscilloscope displaying an induced voltage and the frequency of the field, allowing for the calculation of the magnetic field strength. During this entire process, high flow rate room temperature air (pressurized at 2.5 bar) is applied along the device holder, ensuring that no heat generated from the coil can dissipate to the device or the membrane during experimentation. The temperature of the device components is monitored externally using an infrared thermometer (Thermo Fisher Scientific Inc., USA), also equipped with a temperature probe, to confirm room temperature readings and hence the absence of non-specific heating. Continuous air cooling and temperature control monitoring is performed in such a manner and for every device, during every stage involving inductive heating, to ensure their comparability as proof of concept designs. The third stage repeats the steps performed in stage 2 for the duration of 3 h, with the addition of the activation of the osmotic pump at the start of this step. While ensuring not to agitate the device, the water inlet is wetted with a drop of water, held in place by surface tension with the device in the upright position. The device is then placed in a small water holder used to partially submerge the donor and fully submerge the pump in more water, such that no air remains in the pump's water inlet. The fourth stage consist of a 1.5 h period during which the device is left at room temperature, with the osmotic pump still pressurizing the drug chamber and positioned as described above. The measurements of RhB diffused by the end of each stage are used to determine each stage's average diffusion rate.

The prototype device using the cyanoacrylate treated EC membrane is tested over a span of ∼55 h. First, the device is cycled through three 1 h on-off cycles with the magnetic field applied as described above. In the second stage, the device is cycled through six 1 h on-off cycles with the osmotic pump activated at the start of this step. The third stage consists of leaving the device for 6 h while undergoing osmotic pumping only.

Next, stages 4–7 are obtained by repeating the second and third stages two more times, providing four more data points. The seventh stage (osmotic pumping) is undergone over a 12 h period in contrast to the previous 6 h cycles, to further verify the stability of the state. And finally, the eighth stage consist of a prolonged period of diffusion, over the course of 7 h, with the osmotic pump locked in its deflected position at the end of the seventh stage. To achieve this locked state, the device was removed from the small water holder, the pump's bottom EC membrane was carefully dried with the edge of KimWipes (Kimberley-Clark Corporation, Irving, TX), and the dry water inlet was completely sealed off using a carefully adhered wide area of Kapton tape (DuPont, Wilmington, DE), in contact with the entire bottom and sidewalls of the exterior of the device.

In order to test for non-specific heating during the application of the magnetic field, an experiment is performed with an EC membrane in one case and a CA membrane in another, both fabricated as described in Section II C, but with zero iron oxide content (Figs. 2(a) and 2(c)). Membranes are assembled into the device configuration, and after reaching a steady baseline value of RhB diffusion from the donor chamber to the receptor chamber, the diffusion rates for a 6 h period with no magnetic field application, and a 6 h period with magnetic field application, are measured. Temperature monitoring by infrared thermometer and temperature probe, as well as air cooling, is performed to corroborate the findings. No measurable difference in diffusion rates is observed before and after the applications of the magnetic field for each membrane, and no measureable changes in temperature are observed using the thermometer.

III. RESULTS AND DISCUSSION

A. Individual membrane characterization

The continuous change of absorbance of PNIPAM hydrogels at 500 nm wavelength during heating is shown in Fig. 3(a), where a clear inflection point is observed on the continuous curve. This point indicates that the volume phase transition temperature of tested hydrogels is around 42 °C, which is 5 °C higher than 37 °C human physiological conditions. The chemistry of PNIPAM hydrogels is very well established especially in terms of their thermo-responsivity.[14–24] This concept is applied in this platform where hydrogel particles embedded in the polymer matrix undergo size transition to increase cargo efflux through the heterogeneous membrane. This thermoresponsive size transition is highlighted in Figs. 2(f) and 2(g), where a clear size transition from around 800 nm to 400 nm occurs after heating the hydrogel particles in solution to 45 °C. The same transition is hypothesized to be taking place in the composite membranes. Attempts to capture scanning electron microscopy images of membrane cross sections before and after heating did not clearly show the changes in the embedded hydrogel size, probably due to the packed integration of the hydrogel particles in the polymer matrix.

Using RhB as model drug molecules, diffusion through composite membranes at different temperatures are measured as shown in Figs. 3(b) and 3(c). During 3 h experiments, EC membranes with PNIPAM and SPIO particles diffused at an average rate of 0.28 μg/h, while those at 45 °C diffused at an average rate of 6.65 μg/h. This indicates that the diffusion increases by approximately 24 times when the temperature is increased to 45 °C. For CA membranes with PNIPAM and SPIO particles, the diffusion also increased from room temperature to 45 °C, with the corresponding diffusion rate changing from 1.48 μg/h to 34.14 μg/h, which indicates an increased diffusion of approximately 23 times. Despite the similarity in ratios of ∼23–24 for untreated membranes (Figs. 3(b) and 3(c)), the EC membrane has the lower diffusion rates. This difference between untreated EC and CA membranes is explained by the difference in affinity towards water, as CA is widely considered as hydrophilic while EC as hydrophobic.[61] Furthermore, a study involving water permeability through membranes found that the

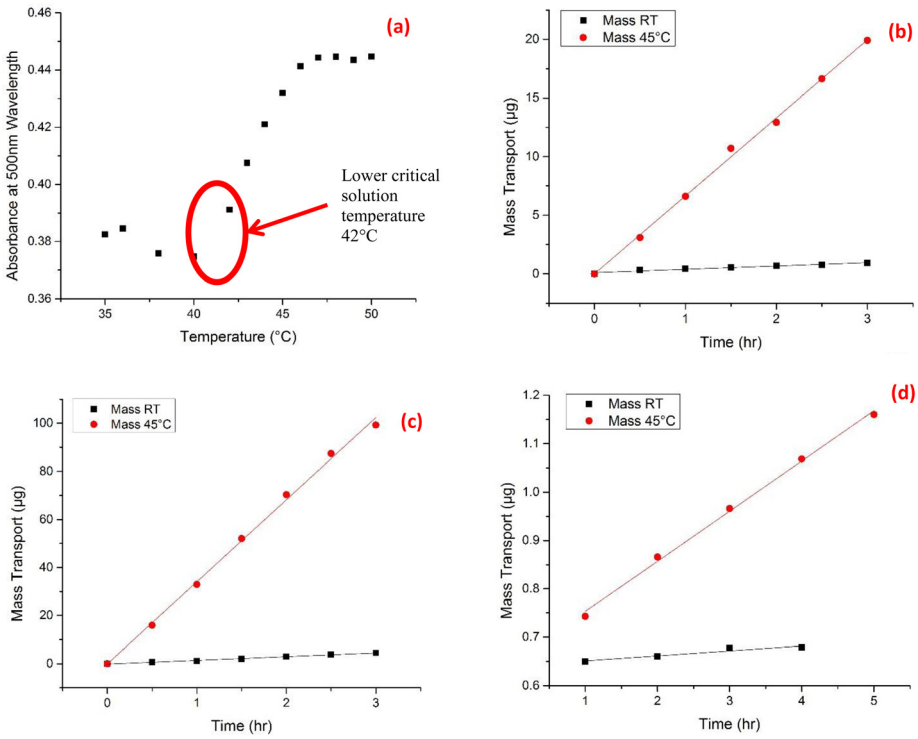

FIG. 3. (a) Absorbance of PNIPAM hydrogels at different temperatures. Diffusion profiles of RhB through (b) EC with PNIPAM and SPIO particles and (c) CA with PNIPAM and SPIO particle composite membranes at room temperature (RT) and at 45 °C. (d) Diffusion profiles of RhB through EC with PNIPAM and SPIO particle composite membranes treated with 0.08 ml of cyanoacrylate (see Methods), at room temperature and at 45 °C.

permeability of EC was less than one fifth that of CA, and could be increased with the addition of another polymer.[62]

Fig. 3(d) shows the diffusion rates measured at room temperature and at 45 °C for a cyanoacrylate treated EC membrane with PNIPAM and SPIO particles. As expected, the addition of the layer impedes the diffusion, resulting in rates of only 0.01 μg/h and 0.1 μg/h, respectively, hence increasing relative diffusion by a factor of 10 with the addition of direct heat over the room temperature state. These rates are measured after a prolonged initial diffusion over several hours to ensure that the smaller amount of RhB passing through the cyanoacrylate-impeded membrane can be detected and reliably measured to generate reported data.

The essential reason for the significant difference between diffusion at <40 °C and that at >40 °C is that the PNIPAM hydrogel occupies different volumes within the diffusion pathways while at these two temperature conditions. At room temperature, owning to the swelling state of the hydrogel while under its transition temperature where the intermolecular H-bonds formed with water increase the volume occupied by hydrogel particles blocking drug pathways, the diffusion is highly inhibited. However, when the temperature increases to 45 °C, high enough to induce the hydrogel's volume phase transition, the intermolecular H-bonds tend to break, while the intramolecular ones are preferred and formed. In this case, the shrinkage of hydrogel particles increases the diffusion pathways around them, resulting in higher diffusion through membranes than that at room temperature. From the diffusion profiles, it is also clear that the thermosensitive behavior of the PNIPAM hydrogel can be maintained no matter which membrane matrix is surrounding it.

Table II summarizes the mean flexural stress at the breaking point, measured for each of the two conditions described, for the mechanical characterization of the two membrane types. CA membranes exhibit larger flexural stress when compared to EC membranes, which is consistent with the experience of a higher failure rate for EC membranes studied. Some EC membranes would crack or leak during device assembly or at the start of diffusion cell testing, while

TABLE II. Mean flexural stress at breaking point for dry and wet CA and EC based membranes. 10 samples measured for each membrane type.

Membrane composition	Mean flexural stress at breaking point (MPa)
CA and PNIPAM, dry	7850 ($\sigma = 825.41$)
CA and PNIPAM wet	7210 ($\sigma = 890.58$)
EC and PNIPAM, dry	5610 ($\sigma = 960.93$)
EC and PNIPAM, wet	3480 ($\sigma = 986.01$)

no CA membranes did so. This suggests that CA is a more mechanically robust polymer to use as a membrane matrix for drug delivery applications, while it only changes the rate by less than an order of magnitude when compared to untreated EC.

B. Controlled release of model drug

In the case of the CA membrane device (Fig. 4(a)), there is a clear increase of rate of diffusion between the room temperature state at 0.48 μg/h (stage A), to the magnetic heating state at 1.41 μg/h (stage B), and the coupled magnetic heating and osmotic pumping state at 1.97 μg/h (stage C). Removal of the magnetic heating, with the pump still on, drops the diffusion rate down to 1.53 μg/h (stage D). Receptor RhB concentration at its maximum is less than 1% of the donor's concentration during experimentation; therefore, the device's results are not significantly affected by the change in concentration of the two solutions.

For the cyanoacrylate treated (0.08 mL evaporation) EC membrane device (Fig. 4(b)), there is a clear increase of delivery rate from 18.9 ng/h in stage A with magnetic heating to 37.2 ng/h in stage B with both magnetic heating and osmotic pumping. Without the magnetic heating but with the active osmotic pump, the delivery rate drops to 28.0 ng/h in stage C. Stages E and G are repetitions of stage C, over two different time intervals (6 h and 12 h), and are in good agreement with the expected value achieved in stage C (27.8 and 27.4 ng/h, respectively). Stages D and F are repetitions of stage B, in which the magnetic field is applied together with osmotic pumping, and demonstrate controllable pulsatile release. And finally, stage H is held for approximately 7 h with only the diffusion process and with neither magnetic heating nor osmotic pumping, resulting in the lowest rate at 11.6 ng/h. All measured diffusion rates are on the nanogram scale and hence receptor concentration falls well below 1%.

C. Simulation-based device characterization and discussion

The overlaid simulation data in Fig. 4 is in good agreement with the experimental results, and supports two important aspects of the analytical approximation, namely, the cubic volume relation and the volume displacement rate relation with the applied pressure (see supplementary material SJ).[63] First, the simulated direct pressure test on the PDMS membrane supports the cubic volume-pressure relation by observing only the PDMS membrane under externally applied pressure. With no magnetic membrane present during this test, a near-linear volume deflection under cubic pressure over time supports the αV^3 term in Equation (3) with reliable accuracy. Under the same condition, the relation pressure $\sim$ time^3 is shown by plotting the applied pressure to the PDMS membrane over time, as well as the relation volume $\sim$ time, by plotting volume deflection of PDMS over time. These two result in the relation pressure $\sim$ volume^3. The results from the direct pressure test support the analytical approximation. The simulation results of the RhB transport through the magnetic membrane over time are plotted along with experimental values, and all simulated parameters, along with derived results, show consistency with experimental values, indicating that the simulation as whole is physically sensible (Fig. 4(b)).

The drug release rate is quite consistent for each magnetic state throughout the simulation: despite the uncertainty in deciding the magnitude of P_{PDMS}, the behavior of the drug delivery and transport rate can be matched and show that with reasonable application of pressure by the

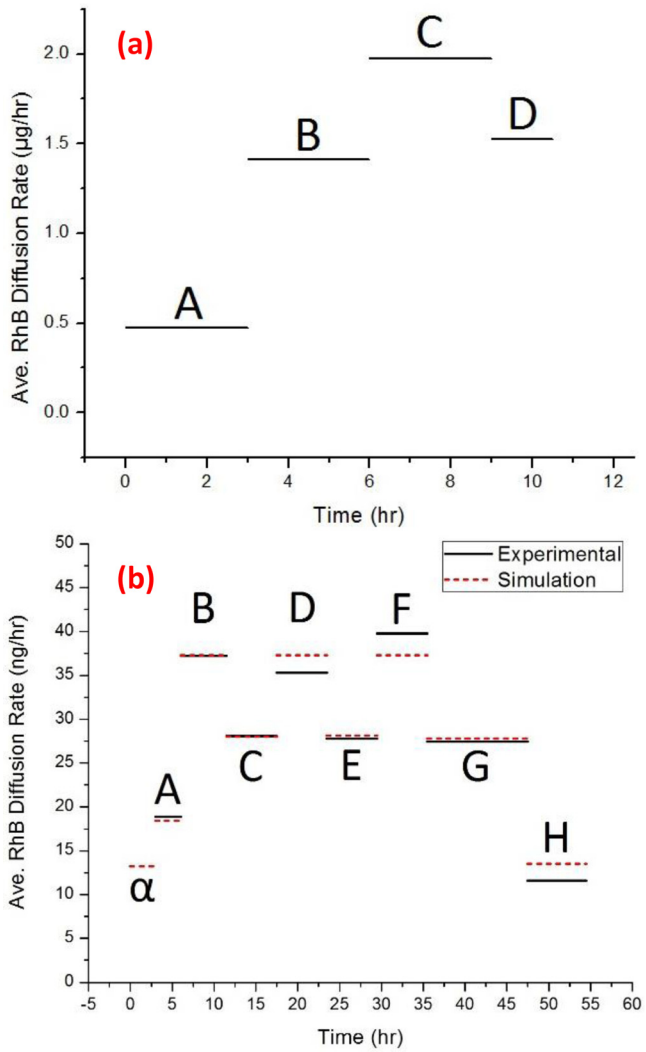

FIG. 4. (a) The CA membrane (cellulose acetate with PNIPAM and SPIO particles) device testing results, with average diffusion rates of RhB sampled for each test stage ((A)–(D)). (A) Room temperature diffusion after reaching steady state baseline value, (B) applied magnetic field (62 mT, 450 kHz, cycled on/off every 30 min) and no osmotic pumping, (C) applied magnetic field (same cycling as in B) with osmotic pumping, (D) osmotic pumping with no applied magnetic field. (b) The cyanoacrylate treated EC membrane (cyanoacrylate treated ethyl cellulose with PNIPAM and SPIO particles) device testing results, with average diffusion rates of RhB sampled for each test stage ((A)–(H)). (A) Applied magnetic field without osmotic pumping, (B, D, F) applied magnetic field with osmotic pumping, (C, E, G) osmotic pumping without applied magnetic field, (H) without magnetic field and locking of osmotic pump in its current deflected position. Red plot indicates simulation results, with point α indicating the simulated value for room temperature diffusion rate, whose mass value is too low to be measured by UV spectrophotometry. Although H is slightly lower than α, it is an experimentally measurable diffusion rate due to the larger amount of RhB present in the receptor chamber.

osmotic chamber, constant drug delivery can be achieved with the complete device setup. While numerical smoothing requires some linear increase and decrease of pressure at the start and end of the osmotic pumping, the pressure profile of the complete device setup is approximately constant throughout the simulation, based on the assumption that the second pressure term in Equation (3) is the dominating term.

While experimentally there is a sharp increase in osmotic pressure in the first few hours once the pumping starts, the general trend of osmotic pressure is to stay at the same pressure, assuming the saturation concentration stays constant. This reasoning is based on the calculation of osmotic pressure using Morse's Law for an ideal, diluted solution. While under the same saturation concentration, the introduction of water should not increase the osmotic pressure. If

there is no undissolved salt precipitate, introduction of water will decrease the molarity of salt water in the osmotic chamber, decreasing osmotic pressure. If there are undissolved salt precipitates, the introduction of water will hold the osmotic pressure constant as more salt is dissolved until the saturation concentration is reached. Thus, the general trend of a rectangular osmotic pressure profile agrees with physical sensibility under Morse's Law of osmotic pressure with an ideal solution. The balance of pressures on the PDMS membrane of the pump supports this pressure profile (see discussion of net forces in supplementary material SG).[63]

The primary purpose of the osmotic pump and the deflection of the PDMS membrane is to provide a back pressure for the small scale diffusion of RhB through the stiff non-flexible magnetic membrane, as illustrated through the simulated dynamics. Though some diffusion occurs without assistance, or can occur with flow assisted diffusion as previously reported,[25] the use of the osmotic pump as a back pressure allows for faster on-off magnetic control of the system, as opposed to using the osmotic pressure as a direct pump for the RhB solution. Furthermore, flow assistance is not possible when implementing the implantable device in vivo, therefore pump assistance is suitable, despite not being used for its maximum pressure potential in displacing the drug volume.

Parameter derivation and estimated values associated with the treated EC composite membrane are summarized in a Table III, along with average RhB transport rates as compared with experimental data.

Porosity and permeability values apply whether or not the pump is active, and as would be expected, shrinking of the hydrogel when heated by magnetic activation causes the porosity and permeability values to increase. However, the simulation results in Fig. 4(b) and Table III show deviations when compared to experimental data since these values are derived from simulation using governing physics and equation that are simplified for simulation efficiency.

Regarding RhB transport rates and parameter determination, simulation results indicate that the drug transport rate seems consistently linear, with constant rate of drug transport per state and stage. Each determined parameter is a constant value for each prescribed state (Table III). This also makes sense physically, as it is likely for values of porosity and permeability to stay constant over time for a given magnetic state.

Calculations of the bending rigidity (D) of both the *pump's* semi-permeable non-magnetic EC membrane ($D_{EC} = 9.5 \times 10^{-7}$ N·m) and the flexible PDMS membrane ($D_{PDMS} = 2 \times 10^{-8}$ N·m) show that the EC membrane is 46 times more rigid than the PDMS membrane. Therefore, the vast majority of the pressure generated by the osmotic pump goes into the pressurization of the donor chamber above the PDMS, as opposed to bending of the semi-permeable membrane. This is evidenced in experiments where, in an individually activated pump, the PDMS membrane is deflected while the semi-permeable membrane appears to be perfectly flat. The magnetic nanocomposite membrane has approximately the rigidity of the bottom membrane, and as such, resists deflection in the face of the pressure transferred to the donor via the PDMS membrane, allowing increased pressure for the diffusion process as opposed to bending of the composite membrane.

TABLE III. Simulation-derived values of porosity (ε) and permeability (k) for the cyanoacrylate treated ethyl cellulose-PNIPAM-SPIO composite membrane, and RhB transport rate of simulated and experimental data.

State	Determined property	Simulated avg. RhB transport (ng/h)	Experimental ave. RhB transport (ng/h)
No pump, magnetic activation	$\varepsilon = 9.70 \times 10^{-5}$ $k = 1.00 \times 10^{-21}$ m^2	18.457	18.894
Pump, magnetic activation	$\varepsilon = 9.70 \times 10^{-5}$ $k = 1.00 \times 10^{-21}$ m^2	39.389	37.464
Pump, no magnetic activation	$\varepsilon = 7.40 \times 10^{-5}$ $k = 0.75 \times 10^{-21}$ m^2	28.343	27.753
All off	$\varepsilon = 7.40 \times 10^{-5}$ $k = 0.75 \times 10^{-21}$ m^2	13.699	11.569

D. Device discussion

The most noticeable difference between the types of membranes used in the devices is with regards to the order of magnitude of the diffusion rates observed in each stage when comparing that of the untreated CA membrane device (μg/h) and that of the cyanoacrylate treated EC membrane device (ng/h). Vibrating sample magnetometer (VSM) measurements confirm that all membranes contain equal amounts of magnetic material.

The differences in diffusion rates (heating versus room temperature with no osmotic pumping) are by a factor of 23–24 when both EC and CA membrane types are tested for their diffusion profiles individually (Figs. 3(b) and 3(c)), 2.9 for the CA membrane device when heated by SPIO particles (Fig. 4(a), points A and B), and 1.6 for the treated EC membrane device when heated by SPIO particles (Fig. 4(b), points A and H). Two possible reasons contribute to this observation: (1) the donor and receptor cells of the devices are not heated during the inductive heating cycles, such that they continuously draw out energy from the membranes, unlike with the direct heating of all solutions surrounding membranes tested in diffusion cells; (2) the distribution of heat supply originating from each magnetic particles (i.e., distributed "points" in space in the membrane) can cause less-uniform shrinkage of PNIPAM hydrogel particles when compared to direct overall heating in diffusion cells. This effect is also present in the stages consisting of osmotic pumping coupled with magnetic heating.

The cyanoacrylate layer applied to the EC PNIPAM SPIO membrane significantly reduces the diffusion rates during all device states. The thin layer partially blocks pores at the top surface of the membrane, increasing the time required for RhB permeation. This approach provides an additional parameter for tuning the magnetic membrane, based on the application's requirements. Results from the untreated CA membrane device (Fig. 4(a)) indicate that magnetic actuation can result in higher drug delivery rate changes than osmotic pumping (points A to B and B to C). This is desirable in practice, since the unvalved osmotic pump is continuously pumping *in vivo*, while the magnetic field is externally controlled. In addition, changing the duration of the duty cycle during the magnetization period can change the relative contributions of the membrane and the pump. However, the large effect of the osmotic pump on the drug delivery rate motivates the implementation of a valve for the osmotic pump's bottom semi-permeable EC membrane to control the pump's osmotic intake of water. In future work, this valve could conveniently be realized by the same magnetic nanocomposite membrane which is used in this work at the outlet of the device, enabling activation of both membranes by the same magnetic field.

Deviations between diffusion rates in stages B, D, and F in Fig. 4(b) may be due to experimental error caused by slight differences in total power output of the inductive heater while generating the magnetic field in cycles. In each on-off cycle, when the field is applied, the power is modulated to a certain percentage of the power output of the machine, and this value stabilizes in slightly different times for each cycle. Such deviation does not apply to stages where the magnetic heating state is not pertinent (hence, stages C, E, and G are almost equivalent).

The use of a cyanoacrylate treatment allows for thin depositions from a vapor that has significant impact on drug release while bypassing limitations regarding casting a membrane at any arbitrarily large thickness, or small hydrogel content, in an attempt to reduce diffusion rates. Such limitation include the following: (i) gravity and surface tension on a cast surface will limit the maximum thickness of the membrane during curing; (ii) the thicker the membrane the more magnetic and hydrogel material is required in order to maintain appropriate heating and pore opening in the z-direction across the entirety of a thicker membrane, while simply treating the membrane with cyanoacrylate can achieve a theoretically limitless amount of impedance without increasing any other materials; (iii) attempting to finely decrease the drug delivery by reducing the porosity of, for example, an already low permeability membrane, is potentially more complicated than a cyanoacrylate treatment because of the risk of dropping below the required percolation for having any flux across the membrane to begin with, while a very thin treatment of cyanoacrylate bypasses any concerns associated with PNIPAM percolation across the membrane.

State of the art magnetic membranes have achieved stimuli-responsive controllability, focusing on different PNIPAM hydrogel types and magnetic membrane thicknesses as design parameters. Findings regarding cyanoacrylate and CA provide additional parameters for tuning drug release rates and for changing the membrane strength, both in an easy fashion. Magnetic membranes have previously never been combined with any type of drug delivery pump or actuator. Furthermore, state of the art osmotic pumps, capable of achieving constant and robust drug release, have not previously been combined with any type of valve system. Therefore, results reported here greatly advance the field of diffusion-based membrane drug delivery by adding a fast acting pressure source. Furthermore, they improve upon reservoir-based, continuous, osmotic drug delivery devices by demonstrating remote modifications of the drug delivery rate.

IV. CONCLUSION

This work is the first to report (i) the realization of the remote control of drug release profiles from integrated devices driven by osmotic pumps, (ii) the demonstration of a more mechanically robust CA membrane matrix, (iii) the treatment of an EC membrane for reducing the drug release rates by approximately a factor of 50 while maintaining the order of the on-off ratio of the devices and bypassing limitations associated with other potential reduction methods, and (iv) the modeling and simulation of the integrated system while in operation. Both novel membrane designs are characterized separately and when implemented in a device. Though traditional EC-PNIPAM based membranes have previously been studied, this study is the first to investigate any kind of PNIPAM based membrane design for its performance while integrated in a functional drug delivery device. The reported drug delivery device enables remote control valving of a pressure driven and diffusion dependent drug and shows the potential for tuning delivery ranges from nanograms to micrograms per hour, while adjusting these ranges post-activation and based on on-demand needs. The magnetically triggerable designs reported here are not limited to coupling with osmotic pumps, but can be implemented with other controllable pressure sources, such as RF pumps,[9,10] which may require the use of stronger membranes such as those made with cellulose acetate.

ACKNOWLEDGMENTS

Research reported in this publication was supported by the King Abdullah University of Science and Technology (KAUST).

Assistance using Instron tool was provided by Dr. Yiqiang Fan, School of Engineering, University of British Columbia, Kelowna, Canada.

[1]E. Nuxoll, Adv. Drug Delivery Rev. **65**, 1611–1625 (2013).
[2]S. Sharma, A. J. Nijdam, P. M. Sinha, R. J. Walczak, X. Liu, M. M. Cheng, and M. Ferrari, Expert Opin. Drug Delivery **3**, 379–394 (2006).
[3]S. Herrlich, S. Spieth, S. Messner, and R. Zengerle, Adv. Drug Delivery Rev. **64**, 1617–1627 (2012).
[4]S. Gupta, R. P. Singh, R. Sharma, R. Kalyanwat, and P. Lokwani, IJCP **6**, 1–8 (2011).
[5]S. Yu-Chuan and L. Lin, J. Microelectromech. Syst. **13**, 75–82 (2004).
[6]F. N. Pirmoradi, J. K. Jackson, H. M. Burt, and M. Chiao, Lab Chip **11**, 3072–3080 (2011).
[7]M. Bäcker, M. Raue, S. Schusser, C. Jeitner, L. Breuer, P. Wagner, A. Poghossian, A. Förster, T. Mang, and M. J. Schöning, Phys. Status Solidi A **209**, 839–845 (2012).
[8]F. N. Pirmoradi, J. K. Jackson, H. M. Burt, and M. Chiao, Lab Chip **11**, 2744–2752 (2011).
[9]Y. Yi, U. Buttner, and I. G. Foulds, Lab Chip **15**, 3540–3548 (2015).
[10]J. Fong, Z. Xiao, and K. Takahata, Lab Chip **15**, 1050–1058 (2015).
[11]Y. Yi, A. Zaher, O. Yassine, J. Kosel, and I. G. Foulds, Biomicrofluidics **9**, 052608 (2015).
[12]N. M. B. Smeets and T. Hoare, J. Polym. Sci. Part A: Polym. Chem. **51**, 3027–3043 (2013).
[13]W.-F. Ma, K.-Y. Wu, J. Tang, D. Li, C. Wei, J. Guo, S.-L. Wang, and C.-C. Wang, J. Mater. Chem. **22**, 15206–15214 (2012).
[14]Y.-H. Lien, J.-H. Wu, J.-W. Liao, and T.-M. Wu, Macromol. Res. **21**, 511–518 (2013).
[15]Y.-H. Lien, T.-M. Wu, J.-H. Wu, and J.-W. Liao, J. Nanopart. Res. **13**, 5065–5075 (2011).
[16]W. Wang, L. Liu, X.-J. Ju, D. Zerrouki, R. Xie, L. Yang, and L.-Y. Chu, ChemPhysChem **10**, 2405–2409 (2009).
[17]J. Rubio-Retama, N. E. Zafeiropoulos, C. Serafinelli, R. Rojas-Reyna, B. Voit, E. Lopez Cabarcos, and M. Stamm, Langmuir: ACS J. Surf. Colloids **23**, 10280–10285 (2007).
[18]Y. Cai and Y.-Y. Liu, Macromol. Chem. Phys. **214**, 882–891 (2013).

[19]N. Lu, K. Yang, J. Li, Y. Weng, B. Yuan, and Y. Ma, J. Phys. Chem. B **117**, 9677–9682 (2013).
[20]Z. Zhu, N. Gao, H. Wang, and S. A. Sukhishvili, J. Controlled Release **171**, 73–80 (2013).
[21]H. D. Han, B. C. Shin, and H. S. Choi, Eur. J. Pharm. Biopharm. **62**, 110–116 (2006).
[22]H. D. Han, M. S. Choi, T. Hwang, C. K. Song, H. Seong, T. W. Kim, H. S. Choi, and B. C. Shin, J. Pharm. Sci. **95**, 1909–1917 (2006).
[23]S. Purushotham, P. E. J. Chang, H. Rumpel, I. H. C. Kee, R. T. H. Ng, P. K. H. Chow, C. K. Tan, and R. V. Ramanujan, Nanotechnology **20**, 305101 (2009).
[24]Y.-L. Yu, M.-J. Zhang, R. Xie, X.-J. Ju, J.-Y. Wang, S.-W. Pi, and L.-Y. Chu, J. Colloid Interface Sci. **376**, 97–106 (2012).
[25]T. Hoare, B. P. Timko, J. Santamaria, G. F. Goya, S. Irusta, S. Lau, C. F. Stefanescu, D. Lin, R. Langer, and D. S. Kohane, Nano Lett. **11**, 1395–1400 (2011).
[26]A. Baeza, E. Guisasola, E. Ruiz-Hernández, and M. Vallet-Regí, Chem. Mater. **24**, 517–524 (2012).
[27]S. H. Hu, Y. Y. Chen, T. C. Liu, T. H. Tung, D. M. Liu, and S. Y. Chen, Chem. Commun. **47**, 1776–1778 (2011).
[28]F. Zhang and C. C. Wang, Langmuir: ACS J. Surf. Colloids **25**, 8255–8262 (2009).
[29]B. Seung-Ki, Y. Yong-Kyu, J. Hye-Seon, S. Soonmin, and P. Jung-Hwan, J. Micromech. Microeng. **23**, 045006 (2013).
[30]B. D. Kieviet, P. M. Schon, and G. J. Vancso, Lab Chip **14**, 4159–4170 (2014).
[31]J. T. Santini, M. J. Cima, and R. Langer, Nature **397**, 335–338 (1999).
[32]A. Hill, S. Breyer, S. Geissler, W. Mier, U. Haberkorn, M. Weigandt, and K. Mader, J. Controlled Release: Off. J. Controlled Release Soc. **168**, 77–87 (2013).
[33]A. Hill, S. Geissler, M. Meyring, S. Hecht, M. Weigandt, and K. Mader, Int. J. Pharm. **451**, 57–66 (2013).
[34]F. Theeuwes and S. I. Yum, Ann. Biomed. Eng. **4**, 343–353 (1976).
[35]R. Farra, N. F. Sheppard, Jr., L. McCabe, R. M. Neer, J. M. Anderson, J. T. Santini, Jr., M. J. Cima, and R. Langer, Sci. Transl. Med. **4**, 122ra21 (2012).
[36]C. N. Patra, S. Swain, J. Sruti, A. P. Patro, K. C. Panigrahi, S. Beg, and M. E. B. Rao, Recent Pat. Drug Delivery Formulation **7**, 150–161 (2013).
[37]X. Zhang, Y. Yi, J. Qi, Y. Lu, Z. Tian, Y. Xie, H. Yuan, and W. Wu, Int. J. Pharm. **452**, 233–240 (2013).
[38]P. A. Tresco and B. D. Winslow, Crit. Rev. Biomed. Eng. **39**, 29–44 (2011).
[39]S. L. DeVos and T. M. Miller, J. Visualized Exp. **76**, e50326 (2013).
[40]W. Martin Bauknight, S. Chakrabarty, B. Y. Hwang, H. R. Malone, S. Joshi, J. N. Bruce, E. Sander Connolly, C. J. Winfree, M. G. Cunningham, J. H. Martin, and R. Haque, J. Clin. Neurosci.: Off. J. Neurosurg. Soc. Australas. **19**, 563–569 (2012).
[41]Y. C. Martins, L. Clemmer, P. Orjuela-Sanchez, G. M. Zanini, P. K. Ong, J. A. Frangos, and L. J. Carvalho, Malar. J. **12**, 138–148 (2013).
[42]X. Liu, T. Terry, S. Pan, Z. Yang, J. T. Willerson, R. A. Dixon, and Q. Liu, J. Visualized Exp. **76**, e50364 (2013).
[43]P. Mulcahy, A. O'Doherty, A. Paucard, T. O'Brien, D. Kirik, and E. Dowd, Behav. Brain Res. **243**, 6–15 (2013).
[44]J. Kost, *Pulsed and Self-Regulated Drug Delivery* (CRC Press, 1990).
[45]J. Wu, K. S. Paudel, C. Strasinger, D. Hammell, A. L. Stinchcomb, and B. J. Hinds, Proc. Natl. Acad. Sci. U.S.A. **107**, 11698–11702 (2010).
[46]N. D. D. Group, Diabetes **28**, 1039–1057 (1979).
[47]D. Mellitus, Diabetes Care **28**, S37 (2005).
[48]G. Bray, E. Gomperts, S. Courter, R. Gruppo, E. Gordon, M. Manco-Johnson, A. Shapiro, E. Scheibel, and M. Lee, Blood **83**, 2428–2435 (1994).
[49]G. C. White, F. Rosendaal, L. M. Aledort, J. Luscher, C. Rothschild, and J. Ingerslev, Thromb. Haemostasis-Stuttgart **85**, 560 (2001).
[50]K. Wolf-Maier, R. S. Cooper, H. Kramer, J. R. Banegas, S. Giampaoli, M. R. Joffres, N. Poulter, P. Primatesta, B. Stegmayr, and M. Thamm, Hypertension **43**, 10–17 (2004).
[51]E. Expert Panel on Detection, JAMA **285**, 2486 (2001).
[52]N. Heart and B. I. N. A. E. P. E. P. O. T. M. O. Asthma, *Guidelines for the Diagnosis and Management of Asthma* (National Asthma Education Program, Office of Prevention, Education, and Control, National Heart, Lung, and Blood Institute, National Institutes of Health, 1991).
[53]M. Asher, U. Keil, H. Anderson, R. Beasley, J. Crane, F. Martinez, E. Mitchell, N. Pearce, B. Sibbald, and A. Stewart, Eur. Respir. J. **8**, 483–491 (1995).
[54]R. S. Fisher, W. V. E. Boas, W. Blume, C. Elger, P. Genton, P. Lee, and J. Engel, Epilepsia **46**, 470–472 (2005).
[55]S. H. Sun, H. Zeng, D. B. Robinson, S. Raoux, P. M. Rice, S. X. Wang, and G. X. Li, J. Am. Chem. Soc. **126**, 273–279 (2004).
[56]Y. J. Lee, G. B. Jung, S. Choi, G. Lee, J. H. Kim, H. S. Son, H. Bae, and H.-K. Park, PLoS One **8**, e79761 (2013).
[57]R. T. Moretti Neto, I. Mello, A. B. Moretti, C. R. Robazza, and A. A. Pereira, Braz. Oral Res. **22**, 43–47 (2008).
[58]S. Timoshenko, S. Woinowsky-Krieger, and S. Woinowsky-Krieger, *Theory of Plates and Shells* (McGraw-Hill, New York, 1959).
[59]S. Whitaker, Transp. Porous Media **1**, 3–25 (1986).
[60]O. K. Teng, Ph.D. thesis, National University of Singapore, 2006.
[61]B. Ding, C. Li, Y. Hotta, J. Kim, O. Kuwaki, and S. Shiratori, Nanotechnology **17**, 4332–4339 (2006).
[62]B. Lindstedt, G. Ragnarsson, and J. Hjärtstam, Int. J. Pharm. **56**, 261–268 (1989).
[63]See supplementary material at http://dx.doi.org/10.1063/1.4931954 for additional information regarding simulation methods and membrane properties.